© 2014. Published by The Company of Biologists Ltd | Development (2014) 141, 929-939 doi:10.1242/dev.103218

RESEARCH ARTICLE

Fascin links Btl/FGFR signalling to the actin cytoskeleton during *Drosophila* tracheal morphogenesis

Pilar Okenve-Ramos and Marta Llimargas*

ABSTRACT

A key challenge in normal development and in disease is to elucidate the mechanisms of cell migration. Here we approach this question using the tracheal system of *Drosophila* as a model. Tracheal cell migration requires the Breathless/FGFR pathway; however, how the pathway induces migration remains poorly understood. We find that the Breathless pathway upregulates *singed* at the tip of tracheal branches, and that this regulation is functionally relevant. *singed* encodes *Drosophila* Fascin, which belongs to a conserved family of actin-bundling proteins involved in cancer progression and metastasis upon misregulation. We show that *singed* is required for filopodia stiffness and proper morphology of tracheal tip cells, defects that correlate with an abnormal actin organisation. We propose that *singed*-regulated filopodia and cell fronts are required for timely and guided branch migration and for terminal branching and branch fusion. We find that *singed* requirements rely on its actin-bundling activity controlled by phosphorylation, and that active Singed can promote tip cell features. Furthermore, we find that *singed* acts in concert with *forked*, another actin cross-linker. The absence of both cross-linkers further stresses the relevance of tip cell morphology and filopodia for tracheal development. In summary, our results on the one hand reveal a previously undescribed role for *forked* in the organisation of transient actin structures such as filopodia, and on the other hand identify *singed* as a new target of Breathless signal, establishing a link between guidance cues, the actin cytoskeleton and tracheal morphogenesis.

KEY WORDS: *Drosophila* tracheal system, FGFR pathway, Fascin, Actin cytoskeleton, Cell migration, Morphogenesis

INTRODUCTION

The development of the *Drosophila* tracheal system is a well-established *in vivo* model for tubulogenesis and cell migration (Affolter et al., 2003; Hogan and Kolodziej, 2002; Lubarsky and Krasnow, 2003). The Breathless (Btl)/FGFR pathway is a key player in tracheal formation and regulates both branch migration and cell diversification (Ghabrial et al., 2003). Whereas Btl targets for cell specification have been identified, much less is known about how Btl signalling is transmitted to direct migration. Btl receptor is activated at the tips of the primary branches by its ligand Branchless (Bnl)/FGF (Klämbt et al., 1992; Ohshiro et al., 2002; Sutherland et al., 1996). Previous reports indicated that Btl activation stimulates filopodia formation, which may promote motility (Ribeiro et al., 2002). However, how Btl triggers filopodia formation and how these filopodia contribute to branch migration remain unclear.

Institut de Biologia Molecular de Barcelona, CSIC, Parc Científic de Barcelona, Baldiri Reixac, 4-8, 08028 Barcelona, Spain.

*Author for correspondence (mlcbmc@ibmb.csic.es)

Received 29 August 2013; Accepted 28 November 2013

Filopodia are dynamic actin-based projections with sensing capacity, playing important roles in adhesion and migration. Filopodia formation requires efficient bundling of actin filaments (Faix et al., 2009; Khurana and George, 2011). Fascins belong to an evolutionary conserved family of proteins that cross-link actin filaments into tightly packed bundles, providing stiffness to different types of actin-based structures, such as microspikes, filopodia, stress fibres or microvilli (Hashimoto et al., 2011; Khurana and George, 2011; Vignjevic et al., 2006). Importantly, fascins have recently received a lot of attention in the biomedical field for their involvement in cancer and metastasis and they are at present tumoral biomarkers emerging as potential therapeutic targets (Hashimoto et al., 2011). A wider understanding of fascin function and regulation, required to design such therapeutic strategies, may come from the analysis of fascin activity in normal conditions in *in vivo* systems. In *Drosophila* there is one single fascin protein, named Singed (Sn). *sn* is required for different actin-based events during fly development, such as blood cell migration, oogenesis or bristle formation (Cant et al., 1998; Tilney et al., 1998; Zanet et al., 2009).

In this study we find that *sn* is transcriptionally upregulated at the tip cells of the tracheal branches in response to the Btl activation, through the effectors Pointed (Pnt) and Anterior open (Aop). We find that this regulation is functionally relevant, as *sn* mediates, at least in part, Btl activity. Our functional analysis indicates that *sn* is required at the tips of the branches, precisely where the Btl pathway is more active, to properly organise the actin cytoskeleton. At the cellular level we find clear defects in filopodia morphology and in the shape of the tip cells in *sn* mutants, and we propose that these defects underlie the defects we observe at the tissue level, including delayed branch migration and terminal cell extension. We find that tracheal formation requires the actin-bundling activity of non-phosphorylated Sn, and that an unphosphorylatable (active) form of Sn is able to promote tip cell features. Finally, we report that during tracheal formation *sn* acts in concert with *forked* [*f*; another actin cross-linker with homology to Espin (Bartles et al., 1996)]. A role for *f* in the organisation of long-lived actin structures such as bristles was previously documented (Tilney et al., 1995); here we unveil for the first time a role for *f* in dynamic filopodia. Taken together, our results provide new insights into how the Btl pathway regulates the actin network and into how this finely tuned bundled actin network regulates tracheal morphogenesis.

RESULTS

Sn accumulates at the tip of the growing tracheal branches

sn was known to be expressed in different embryonic tissues (Zanet et al., 2009), and Berkeley Drosophila Genome Project reported expression in the tracheal system, suggesting a tracheal requirement.

Our analysis of Sn protein accumulation indicated a spatially regulated pattern in the trachea. Sn accumulated highly at the tips of the primary branches from stage 12 (Fig. 1B). At stages 13 and 14 Sn accumulated strongly in the tip cells of the dorsal trunk (DT),

Development (2014) doi:10.1242/dev.103218

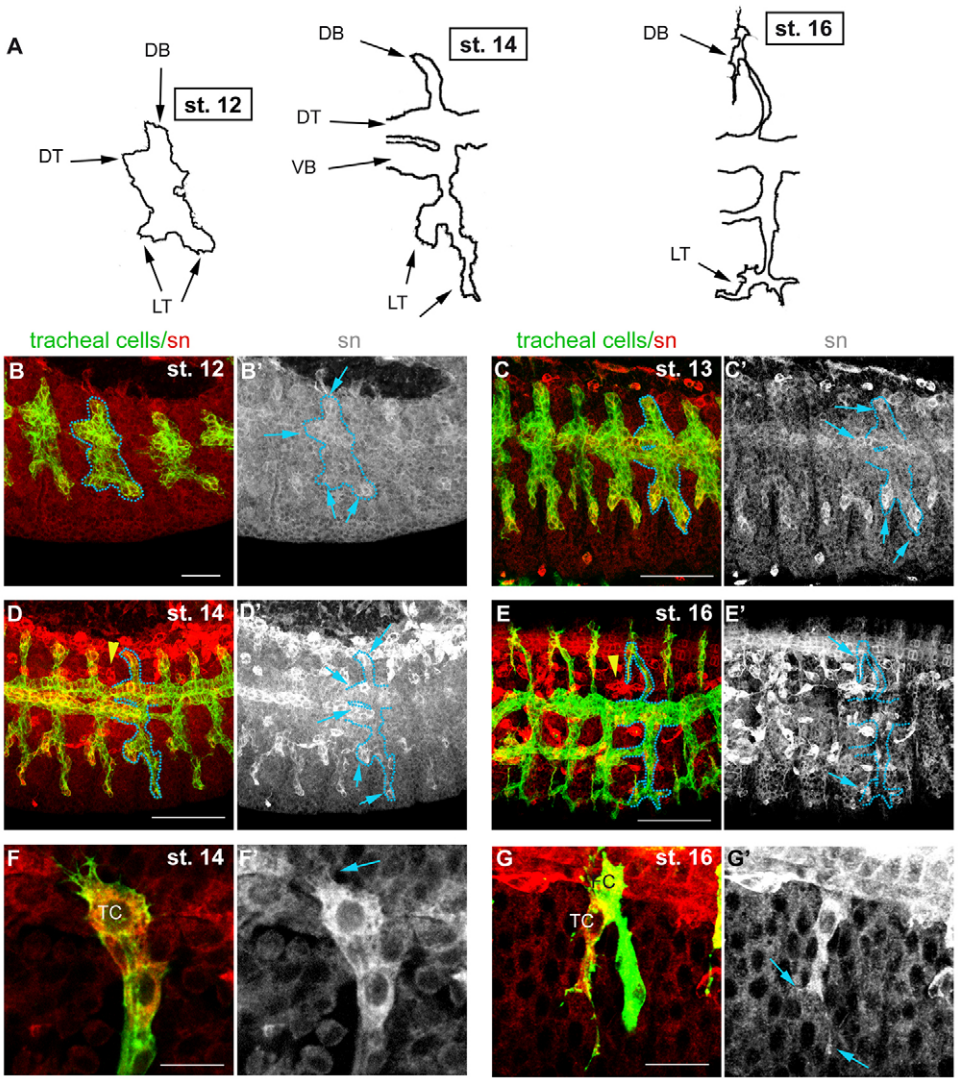

Fig. 1. Accumulation of Sn protein during tracheal development.
(A) Schemes of tracheal metameres. (B-G′) Wild-type embryos at indicated stages stained for green fluorescent protein (GFP; green) to show tracheal cells and for Sn (red or white). In B-E′, blue arrows point to increased accumulation of Sn at the tips of the branches indicated in A. Yellow arrowheads point to plasmatocytes. In F-G′, arrows point to filopodia of terminal cells of dorsal branches. Scale bars: 25 µm in B; 50 µm in C-E; 10 µm in F,G. DB, dorsal branch; DT, dorsal trunk; FC, fusion cell; LT, lateral trunk; TC, terminal cell; VB, visceral branch.

dorsal branches (DB), lateral trunk (LT) and most cells of the visceral branch (VB) (Fig. 1C,D,F). By stage 15 high Sn levels were restricted to the one or two cells nearest the tip in each branch, and this pattern was maintained until late stage 16 (Fig. 1E,G). Besides this enhanced accumulation, Sn also accumulated at lower or basal levels in all tracheal cells throughout development. At the subcellular level we observed a cytoplasmic accumulation of Sn, including the specialised actin-rich filopodia (Fig. 1F,G).

A PlacZ reporter of *sn* expression (sn^{P1}) showed comparable patterns of expression and protein accumulation (supplementary material Fig. S1), indicating that *sn* is transcriptionally regulated during tracheal development.

sn is a target of the Btl/FGFR pathway

The Btl pathway is activated by its ligand Bnl/FGF at the tips of tracheal branches (Klämbt et al., 1992; Ohshiro et al., 2002; Sutherland et al., 1996). The correlation between Sn pattern and Btl activation suggested that *sn* is a target of Btl. Consistent with this we observed that loss of *bnl* prevented high accumulation of Sn in tracheal tip cells, whereas the pattern elsewhere (e.g. in plasmatocytes) was unaffected (Fig. 2A). Conversely, *bnl* tracheal misexpression led to high levels of Sn in all tracheal cells (Fig. 2B).

Btl signals through the Ras-MAP kinase pathway and controls transcription through the transcription factor Pnt (Cabernard and Affolter, 2005; Samakovlis et al., 1996a). However, it was also shown that Btl can signal in the trachea in a Pnt-independent manner (Ribeiro et al., 2002). *pnt* is expressed in the trachea in a pattern comparable to that of *sn* (Fig. 2C,D), suggesting that *sn* is a target of *pnt*. The pattern of Sn in the absence or generalised expression of *pnt* (Fig. 2E,F) confirmed this hypothesis.

In contrast to Pnt, the transcription factor Aop is inactivated by the Btl pathway and negatively regulates Btl activity by competing with Pnt for ETS binding sites (Ohshiro et al., 2002). Accordingly, we found that *aop* negatively controls *sn* expression (Fig. 2G,H).

Collectively our results show that *sn* expression is regulated by the Btl pathway through the nuclear effectors Pnt and Aop. The use of the reporter allele showed that this regulation is transcriptional (supplementary material Fig. S1).

sn and *bnl* genetically interact during tracheal formation

Our results showed that the Btl pathway regulates *sn* expression. To confirm the functional relevance of this regulation we carried out genetic interactions. *bnl* is a haploinsufficient locus with two-thirds of the heterozygotes showing branching defects (Sutherland et al., 1996). We took advantage of this sensitised background and asked whether we could modify the phenotype by modulating *sn* activity. In *sn* mutants, as in the wild type, 20 ganglionic branches (GBs) entered the ventral nerve cord (VNC), while in *bnl* heterozygotes

Development (2014) doi:10.1242/dev.103218

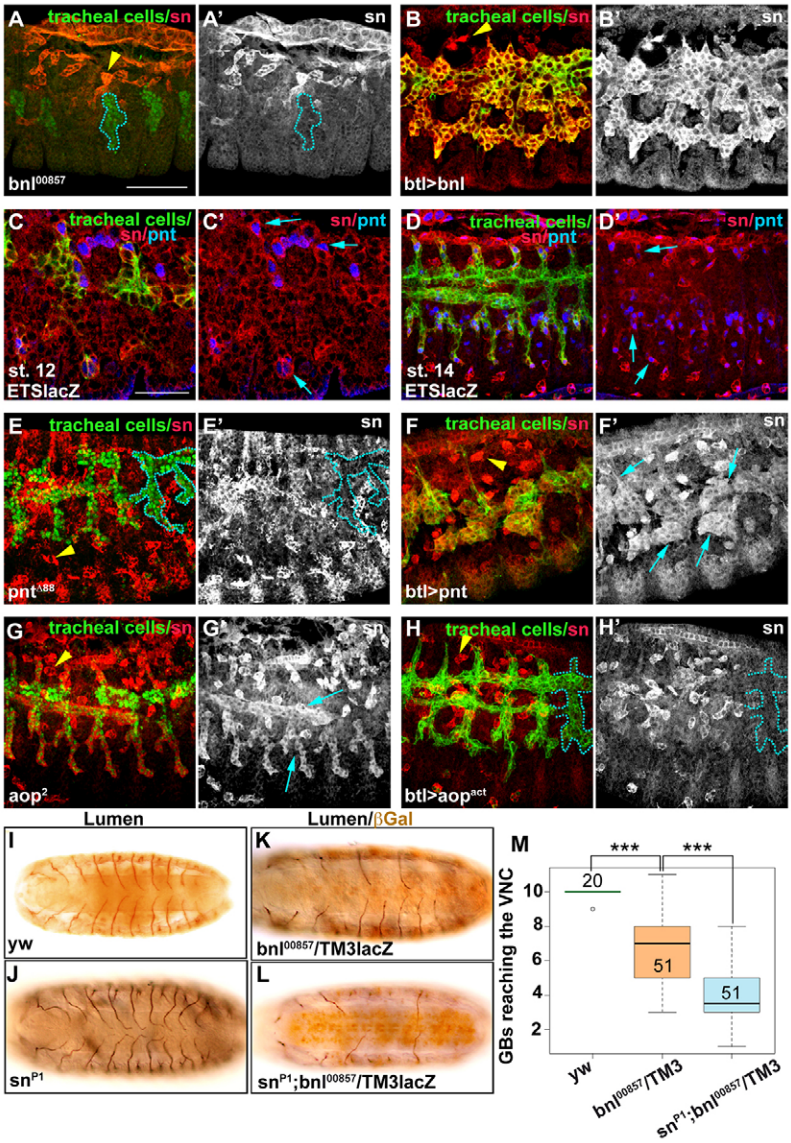

Fig. 2. The Btl pathway regulates Sn expression. (A-H) Stage 14-15 (unless otherwise stated) embryos stained for tracheal cells (green) and Sn expression (red and white). Blue arrows point to increased Sn accumulation. Outlined metameres show no Sn upregulation. Yellow arrowheads point to plasmatocytes. (C,D) Sn and Pnt (blue, assayed by β-gal expression) colocalise at tip cells. In loss of *bnl* and *pnt* function, Sn is not accumulated in tracheal cells (A,E), whereas their misexpression leads to a generalised increased accumulation of Sn (B,F). Aop shows the opposite regulation of Sn expression (G,H). (I-L) Ventral views of embryos showing ganglionic branches (stained for 2A12) entering the ventral nerve cord. (M) Quantification of the number of ganglionic branches entering the ventral nerve cord. Scale bars: 50 μm in A; 25 μm in C. GB, ganglionic branch; VNC, ventral nerve cord.

only 6.9 GBs out of 20 GBs entered (n=51 embryos). These GB defects of *bnl* heterozygotes were significantly increased when *sn* activity was downregulated, and only 3.6 GBs entered the VNC (Fig. 2I-M) (n=51 embryos). This result indicates that *bnl* and *sn* interact, suggesting that *sn* modulates *bnl*-mediated cell migration.

Functional analysis of *sn* in the trachea

We characterised *sn* tracheal requirements in DBs. Because *sn* is required during oogenesis (Cant et al., 1994), we could not analyse the complete lack of Sn (maternal and zygotic). Alternatively, we analysed maternal and zygotic hypomorphic mutants (sn^{P1}, viable and fertile), zygotic amorphic mutants (sn^{28}, viable and female sterile), and homozygous hypomorphic females crossed to amorphic males (sn^{28}/sn^{P1}). Loss of *sn* activity in these combinations was confirmed by absence of Sn (supplementary material Fig. S2 and not shown). *sn* downregulation produced defects at the tips of the branches (see following subchapters), where *sn* levels are high and Btl activity is maximal.

sn is required for DB extension and pathfinding

sn mutants displayed defects in branch pathfinding as many DBs were misguided and often contacted the adjacent ones (Fig. 3A-C; supplementary material Movie 2). In addition, we found cases of branch outgrowth delays. To investigate a requirement for *sn* in branch extension we performed time-lapse analyses to measure the approaching of contralateral wild-type DBs in dorsal views until they meet at the dorsal midline (Fig. 3D; supplementary material Movie 1). We plotted the distance separating each pair of contralateral DBs independently with respect to time and extracted the speed of approaching as a measure of branch extension. We found that the average speed ranged from 0.66 to 0.81 μm/minute between DB4 and DB7 (Fig. 3F shows DB4 results). A comparable analysis of *sn* mutants indicated that the absence of *sn* slows down the speed of migration (from 0.54 to 0.61 μm/minute between DB4 and DB7) (Fig. 3E,F; supplementary material Movie 2), indicating defects in DB extension.

sn is required for terminal branching

Terminal branches, which arise from terminal cells expressing Dsrf (Bs – FlyBase) (Guillemin et al., 1996), form at the tips and require Btl activity (Samakovlis et al., 1996a). In *sn* mutants we detected three different types of terminal branching defects: extra terminal branches, defects and delays in terminal branch extension, and misguidance of terminal branch lumina (Fig. 4A-J).

Development (2014) doi:10.1242/dev.103218

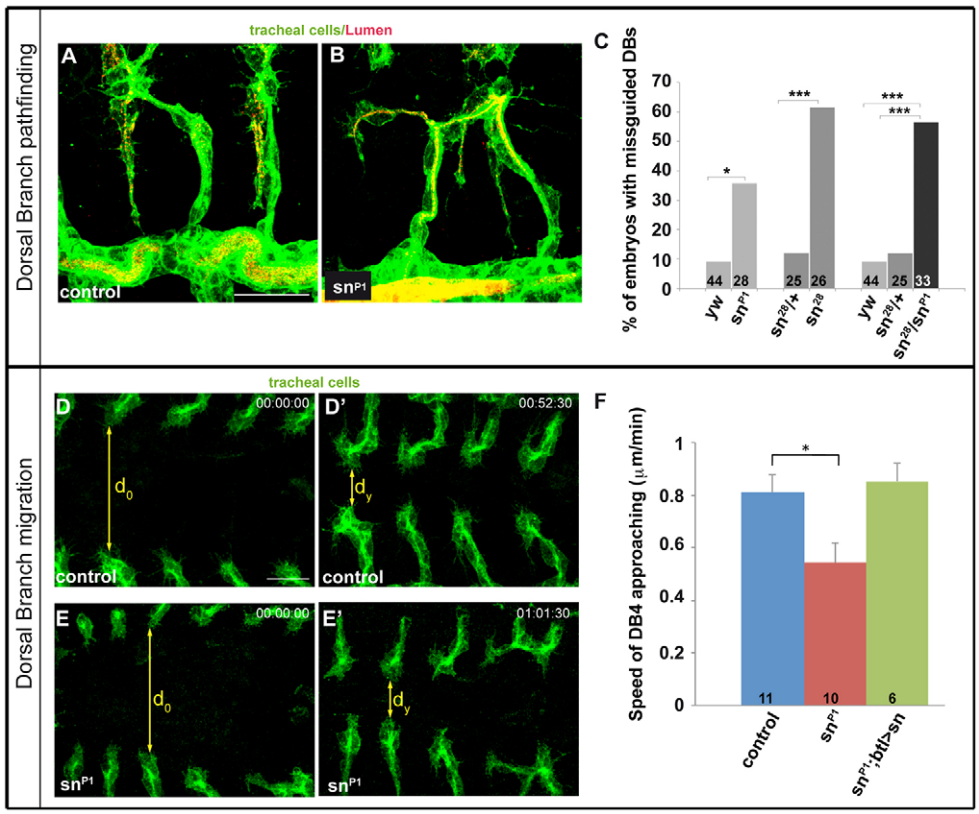

Fig. 3. *sn* requirements in branch pathfinding and migration. (A,B) Two adjacent DBs of stage 16 embryos stained for tracheal cells (green) and lumen (red). Note the DB misguidance and the ectopic fusion with an adjacent DB in *sn* mutants. (C) Quantification of DB misguidances in different genetic backgrounds. (D,E) Images from time-lapse showing the approaching of DBs in dorsal views. Note the delay (time is indicated) in *sn* mutants to reach the same DB contralateral distance. (F) Speed of DB approaching of metamere 4. Note the delay in branch migration in *sn* mutants and the rescue when *sn* is added back. Numbers inside bars correspond to number of embryos analysed (n). Error bars indicate s.e. s.d.: control 0.22; sn^{P1} 0.26; sn^{P1};*UASsn* 0.15. Scale bar: 25 μm.

The extra terminal branches arose from extra Dsrf-expressing cells (Fig. 4B), indicating that *sn* is directly or indirectly involved in tracheal identity specification. To better characterise the two other terminal branching defects, we resorted to *in vivo* analyses. In wild type, DB terminal cells typically extend a cytoplasmic projection directed ventrally during the approaching of contralateral branches. This growing projection accommodates and directs the formation of a new intracellular lumen (Gervais and Casanova, 2010; Kato et al., 2004; Oshima et al., 2006) (Fig. 4F,H; supplementary material Fig. S3A, Movie 3). In *sn* mutants, the ventral cytoplasmic projection was often delayed and extended only during or after contact of contralateral branches. In addition, the lumen was often misguided, generating bifurcated or turned terminal branches (Fig. 4G,I; supplementary material Fig. S3B, Movie 4). These results indicated that *sn* participates in the cellular events required to extend and direct terminal branches.

sn is required for DB fusion

Branch fusions that connect the tracheal network are mediated by the specialised fusion cells (Gervais et al., 2012; Lee et al., 2003; Lee and Kolodziej, 2002; Samakovlis et al., 1996b; Tanaka-Matakatsu et al., 1996), which also accumulate high levels of Sn (Fig. 1G). In *sn* mutants, both the penetrance and expressivity of DB fusion defects were increased when compared with wild type (Fig. 4N). These defects were not due to an incorrect specification of fusion cells, as the fusion marker Dysfusion (Dys) (Jiang and Crews, 2003) was normally expressed (Fig. 4K,L). In wild-type embryos fusion cells first emit filopodia towards each other (Gervais et al., 2012; Samakovlis et al., 1996b; Tanaka-Matakatsu et al., 1996) and then extend a polarised cytoplasmic process that initiates a broader cell contact (supplementary material Fig. S3C, Movie 3). Later, a new structure organised by E-cadherin and the actin cytoskeleton forms at the contact point and assists the formation of the penetrating lumen (Lee et al., 2003; Lee and Kolodziej, 2002). We detected different defects in *sn* mutants that result in a lack of DB fusion: branch misguidance (as already described); formation of an irregular cytoplasmic process, which seemed inefficient to promote and/or maintain a full contact of fusion cells (supplementary material Fig. S3D, Movie 4); formation of a faint track of actin (Fig. 4M). In summary, *sn* downregulation leads to branch fusion defects derived from different abnormalities, which can be attributed to defects in guided migration and cell contact.

sn is autonomously required in the tracheal system

Two sets of experiments confirmed an autonomous requirement of *sn* in the trachea: (1) adding back *sn* in the tracheal system rescued branch fusion, terminal lumen guidance or branch extension (Fig. 3F, Fig. 4E,J,N, Fig. 6C,J); (2) the tracheal expression of *sn* RNAi (which decreased Sn in the trachea, supplementary material Fig. S2) produced tracheal defects comparable to those observed in *sn* mutants (Fig. 4E,J,N) and increased the defects in DB fusion in a *sn* mutant background (Fig. 4N).

sn regulates filopodia and morphology of tracheal cells

We aimed to understand the cellular basis of the aforementioned tissue defects of *sn* mutants. Fascins organise actin-based structures, such as filopodial extensions (Hashimoto et al., 2011). Because filopodia form at the tip of tracheal branches in response to Btl (Ribeiro et al., 2002), precisely where Sn levels are higher, we investigated whether *sn* regulates this filopodial activity. High-resolution time-lapse analysis (10 seconds/frame) in the wild type indicated that these filopodia are very dynamic (Fig. 5A; supplementary material Movie 5). Morphologically, these filopodia are straight, perpendicular to the membrane and display a stiff appearance. Interestingly, we also noticed that the dynamics of these filopodia correlated with the advance of lamellipodia-like cell fronts,

Development (2014) doi:10.1242/dev.103218

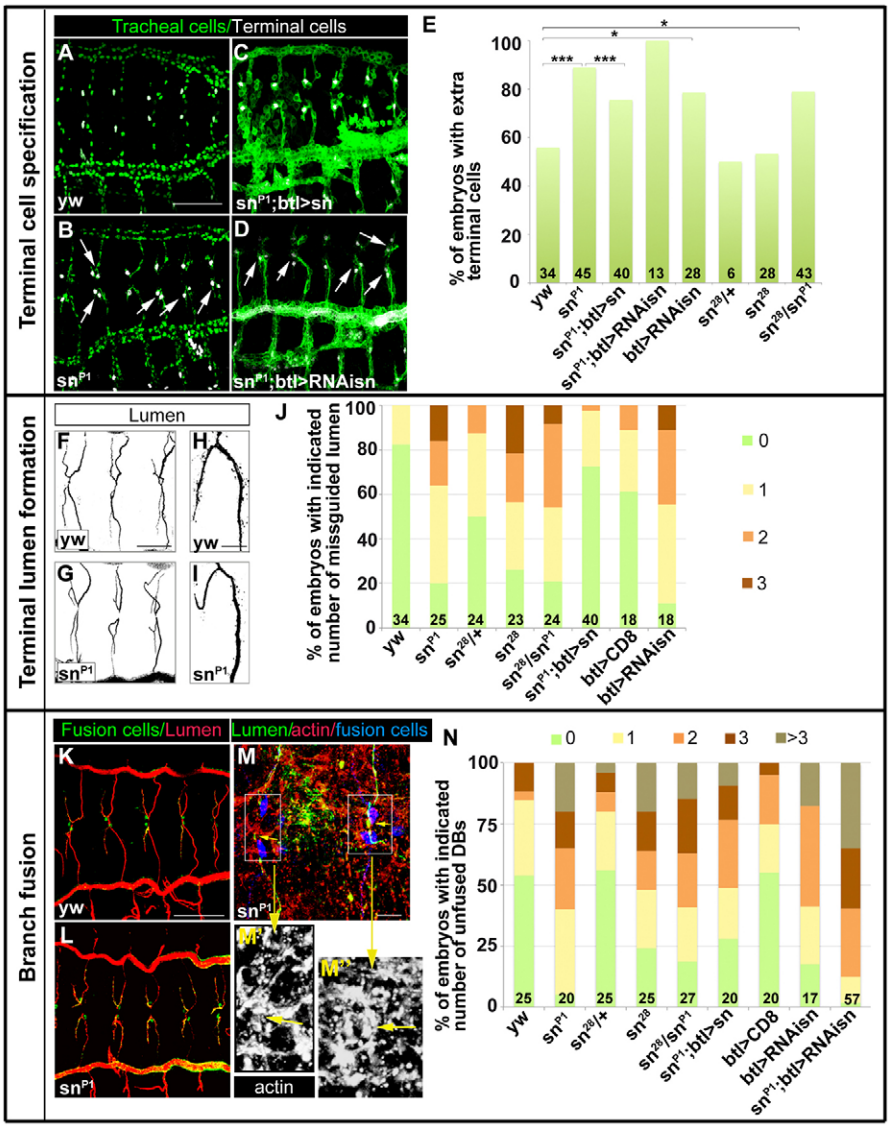

Fig. 4. *sn* requirements in terminal branching and branch fusion. (A-D) Stage 16 embryos showing the tracheal cells (green) and Dsrf as a marker of terminal-cell specification (white). Arrows point to extra terminal cells. (E) Quantification of the penetrance of the terminal-cell specification defects. (F-I) Details of one (H,I) or three pairs (F,G) of DBs at stage 16 in embryos stained for 2A12. (J) Penetrance and expressivity of the terminal lumen guidance defects in the genetic backgrounds indicated. Colours indicate the number of defects per embryo. (K-M) Stage 16 embryos marked for 2A12 (red in K,L, green in M) and Dys (green in K,L, blue in M). Actin staining (red or white in M) shows the formation of a normal actin track in some cases (M″ inset) and an abnormal one (M′) in others. (N) Penetrance and expressivity of fusion. Colours indicate the number of defects per embryo. Numbers inside bars correspond to number of embryos analysed (n). Scale bars: 25 µm in A,F,K; 7.5 µm in H,M.

so that dense filopodial activity anticipates the formation of organised cytoplasmic processes. For instance, the angle of a prominent pool of filopodia directed dorsoanteriorly correlates with the direction of migration of the branch (see Materials and Methods), suggesting a role in directed migration. By contrast, a dorsally directed pool correlates with branch fusion. Finally, a ventrally directed pool anticipates the formation of the cell extension that will generate the terminal branch (supplementary material Movies 3, 5).

In *sn* mutants we observed a similar pattern to that of the wild type in terms of length and direction of filopodia extensions, but a decrease in the number (Fig. 7F,G). We also noticed a fully penetrant phenotype in *sn* mutants: filopodia were curved or wavy (the presence of curved filopodia was five times higher than in controls; see Materials and Methods), often parallel to the membrane and with a flaccid appearance. These consistent filopodia defects were accompanied by the irregular advancement of cytoplasmic processes or cells fronts that resulted in abnormal tip cell shapes (Fig. 5B; supplementary material Movie 6). Our results show that Sn controls the morphology of Btl-regulated actin-based filopodia at tracheal tips and suggest that these filopodia may contribute to sustaining fully organised lamellipodia-like cytoplasmic processes.

Sn regulates actin organisation at the tracheal tips

To analyse the organisation of the actin cytoskeleton, we visualised F-actin in fast time-lapse movies by expressing Utrophin-Green fluorescent protein (UtrGFP) in the tracheal cells. UtrGFP revealed a well-organised cortical actin network formed by long and persistent actin ribs or microspikes probably formed by actin bundles. These actin microspikes arise inside the cytoplasmic processes of the tip cells (which we therefore define as a lamellae) and protrude beyond the cell front forming the filopodia. In addition, a dense, thick and persistent actin mesh organises at the front of the tip cell, which can be defined as lamellipodia (Fig. 5D; supplementary material Movie 7). By contrast, in *sn* mutants, the actin network was disorganised: (1) instead of long actin ribs from the lamellae we found actin accumulated in punctae or short filaments that hardly extend through the lamellipodium or filopodial bases; (2) the lamellipodial actin meshwork was weakly and transiently organised (Fig. 5E; supplementary material Movie 8). Similar results were obtained when Moesin-GFP (MoeGFP) was used to visualise the actin network (supplementary material Fig. S4). Thus, our results show an abnormal organisation of the actin network in *sn* mutants consistent with a defective bundling of actin filaments that would lead to inefficient migratory lamellipodia as well as to flaccid and bent filopodia.

Development (2014) doi:10.1242/dev.103218

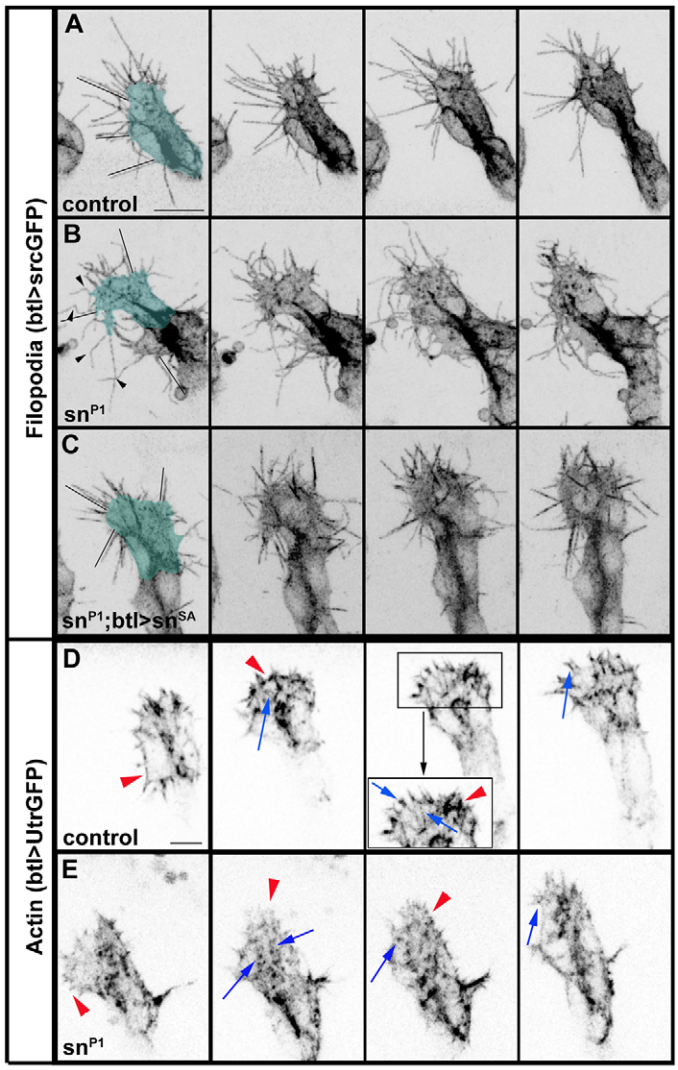

Fig. 5. *sn* is required for cell shape and filopodia morphology and for proper actin organisation. Time-lapse images of DB tip cells at stage 15. (A-C) Filopodia (visible with btl>srcGFP) are bent and flaccid in *sn* mutants (arrowheads in B) and cell fronts are irregular. These defects are rescued by sn^{SA} (C). Thin lines parallel to filopodia reveal filopodia straightness. (D,E) Actin network visualised with btl>UtrGFP. Note the actin ribs protruding towards the filopodia (blue arrows) and the thick cortical meshwork at the lamellipodia (red arrowhead) in the wild type (D). In *sn* mutants (E) this actin organisation is abnormal. Scale bars: 10 µm in A; 5 µm in D.

Sn activity in tracheal formation is regulated by phosphorylation

Sn bundling activity is controlled post-transcriptionally by phosphorylation on Serine 52 (in flies)/39 (in vertebrates) (Tilney et al., 2000; Vignjevic et al., 2006; Yamakita et al., 1996; Zanet et al., 2009). Accordingly, a phosphomimetic form of Sn (Sn^{S52E}) cannot provide the *sn*-bundling activity required for bristle formation in *Drosophila*, whereas the non-phosphorylatable form (Sn^{S52A}) can perform such activity, indicating that S52 phosphorylation inactivates Sn. However, in other tissues (plasmatocytes and nurse cells), S52 phosphorylation does not inactivate Sn (Zanet et al., 2009). We asked whether phosphorylation on S52 is important for tracheal formation.

We expressed sn^{S52E} and sn^{S52A} in wild-type tracheal cells. Overexpression of sn^{S52A} produced defects in branch fusion, and, remarkably, ameliorated unspecific defects in DB pathfinding and terminal branching observed in control embryos (Fig. 6A,B and not shown). By contrast, the phenotypes of sn^{S52E} were in line with loss of *sn* function and produced defects in terminal branching and fusion (Fig. 6A,B). This result indicates that Sn^{S52E} acts as a dominant negative. It has been shown that fascin active and inactive conformations exist in equilibrium, regulated by interactions with actin (Yang et al., 2013). The overexpression of Sn^{S52E} must somehow displace this equilibrium towards the inactive form.

To more clearly assess the activity of each phosphovariant, we tested their capacity to rescue *sn* endogenous downregulation. Consistent with dominant-negative activity, Sn^{S52E} exacerbated several *sn* tracheal defects, such as branch fusion failure (Fig. 6A) or the speed of branch extension (Fig. 6C). At the cellular level we observed stronger defects than in *sn* mutants, such as very abnormal cytoplasmic extensions at tip cells (Fig. 6K). Conversely, sn^{S52A} rescued most aspects of *sn* phenotype at the tissue level, including branch extension, fusion and terminal branching defects (Fig. 6A-C), as wild-type *sn* does (Fig. 4J,N, Fig. 6C,J,). At the cellular level, sn^{S52A} also rescued the formation of straight filopodia, further confirming the tracheal autonomous requirement of *sn* (Fig. 5C). This correlated with an increased accumulation of actin detected along the length of filopodia, as observed in time-lapse imaging (supplementary material Fig. S4C). In addition, tip cells formed prominent and thick cytoplasmic extensions that often arose slightly earlier than in wild-type embryos (Fig. 6G,J). Strikingly, tip cells appeared very often clearly clustered in an advanced position connected to the rest of the stalk cells by a narrow bottleneck, and these clusters sometimes contained more cells (arrows in Fig. 6G; supplementary material Movie 9). These results unveil a dominant effect of Sn^{S52A}, and indicate that it can promote migratory and protrusive tip cell features.

We analysed the subcellular accumulation of Sn^{S52E} and Sn^{S52A} proteins. Although both proteins accumulated in the cytoplasm and in projections, we detected an enrichment of Sn^{S52A} in filopodia protrusions, whereas Sn^{S52E} accumulated more diffusely in the cytoplasm (Fig. 6D,E; supplementary material Movies 10, 11). These results are consistent with a correlation between the activity, accumulation and phosphorylation state of Sn (Nagel et al., 2012; Zanet et al., 2012).

sn and *f* interact during tracheal formation

Most actin-based structures are assembled by more than one actin cross-linker (Khurana and George, 2011). In *Drosophila*, bristle formation requires both *sn* and *f* (Tilney et al., 2003; Tilney et al., 1998; Tilney et al., 1995). We investigated whether F cooperates with Sn in the trachea.

We detected additive effects in branch fusion in sn^3f^{36} double mutants (Fig. 7E). We also detected synergistic interactions, as a proportion of double mutants showed defects not observed in single mutants alone (Fig. 7A-D). In particular, we detected lack of DBs (in 71% of embryos, n=46, Fig. 7D) and lack of terminal branches (in 100% of embryos, n=14, Fig. 7C). Stainings for Dsrf showed lack of terminal cells in all embryos analysed (from two to six Dsrf cells missing per embryo, n=14; Fig. 7C). The absence of Dsrf-expressing cells partially explains the lack of terminal branches, but we also found examples in which the terminal cell was correctly specified and yet the terminal branch was shorter or defective (arrows in Fig. 7C).

Synergistic interactions between two genes usually reflect the fact that they are functionally related. In agreement with this hypothesis,

Development (2014) doi:10.1242/dev.103218

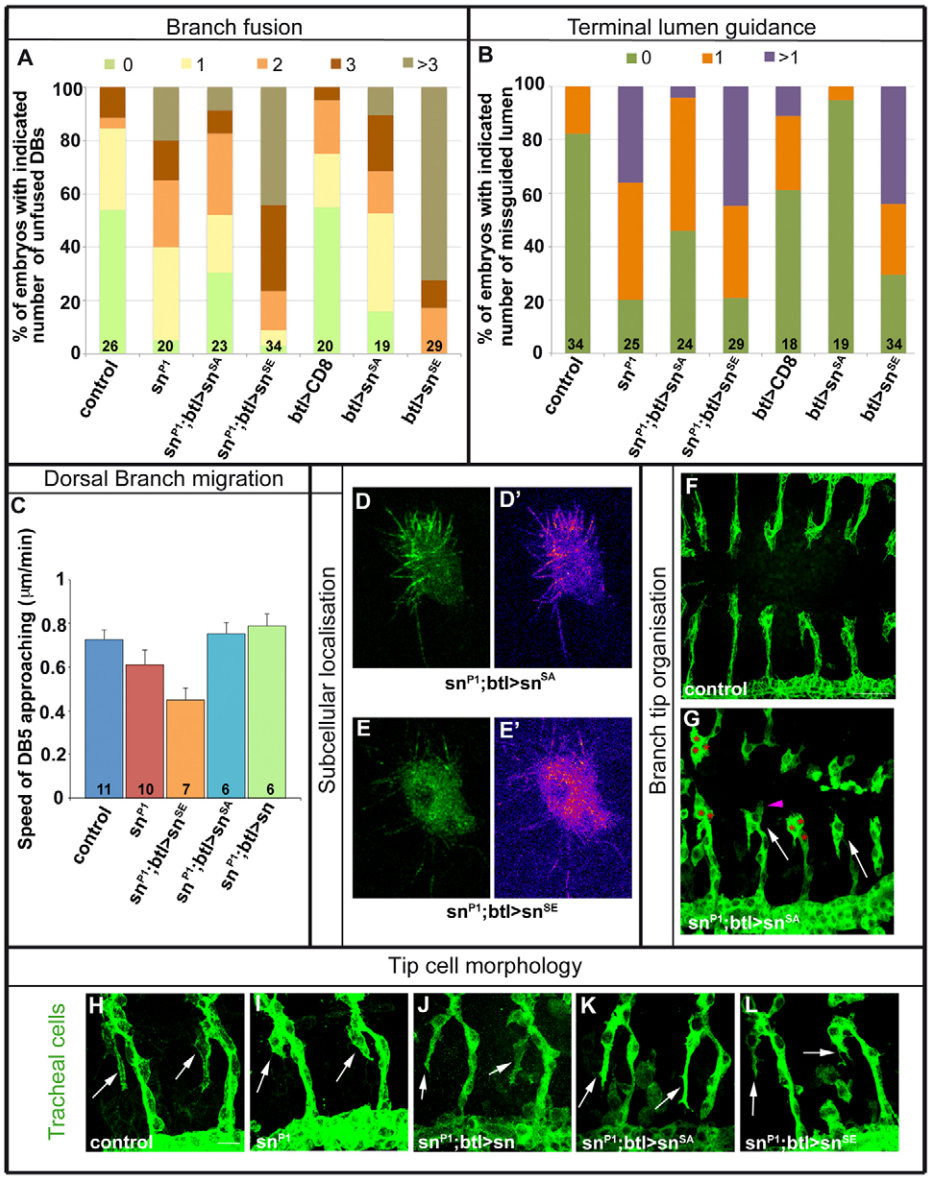

Fig. 6. Tracheal requirements of S52 phosphorylation. (A,B) Penetrance and expressivity of branch fusion and terminal lumen guidance defects in the genetic backgrounds indicated. Colours indicate the number of defects per embryo. (C) Speed of DB approaching of metamere 5. Note the increased delay in migration with respect to *sn* in the presence of sn^{SE} and the rescue with sn^{SA}. Error bars indicate s.e. s.d.: control 0.14; sn^{P1} 0.22; sn^{P1};*UAS*sn^{SE} 0.14; sn^{P1};*UAS*sn^{SA} 0.12; sn^{P1};*UASsn* 0.12. (D,E) Time-lapse images of sn^{SE} and sn^{SA}-GFP constructs showing enhanced GFP accumulation in filopodia in sn^{SA} and cytoplasmic accumulation in sn^{SE}. Pseudocoloured images alongside (D′,E′) facilitate visualisation of subcellular accumulation. (F,G) Stage 15 embryos showing tracheal cells (green). Overexpression of sn^{SA} leads to clustered and advanced tip cells (white arrows), occasional excess of tip cells (red asterisks marking more than the normal two tip cells), and prominent cytoplasmic extensions (pink arrowhead). (H-L) Details of two adjacent DBs at stage 16 (right after branch fusion). Note the differences in terminal cell extension (arrows) and branch fusions. Numbers inside bars correspond to number of embryos analysed. Scale bars: 25 µm in F; 10 µm in H.

we find that both *f* and *sn* mutants alone display bent and wavy filopodia. In addition, filopodia quantifications in double mutants showed significant differences with control embryos and with each mutant alone. In particular, whereas in *f* mutants filopodia were shorter and in *sn* mutants were decreased, in double mutants they were very strongly decreased and short (Fig. 7F,G). Time-lapse imaging confirmed that double mutants extended only few and short filopodia, which displayed a curved and flaccid aspect. In addition, the cytoplasmic processes and consequently the shape of tip cells were more affected than in single mutants (Fig. 7H; supplementary material Movie 12). Thus, our results reveal a previously undescribed role of F in embryogenesis, acting in concert with Sn to regulate the actin cytoskeleton in the tracheal tissue. Accordingly, we found that *f* is expressed in a general pattern, including tracheal cells (supplementary material Fig. S5).

To gain insight into the molecular mechanisms of *sn* and *f* interaction we assayed the ability of *sn* to rescue $sn^{3}f^{36}$ defects. We found a rescue of filopodia morphology and of tip cell shape (Fig. 7I; supplementary material Movie 13), indicating that Sn can overcome the requirement of F when it is overexpressed.

DISCUSSION

sn is a target of Btl/FGFR activity

The FGFR pathway is an essential regulator of many cellular activities (Brooks et al., 2012). In *Drosophila*, the Btl/FGFR pathway stimulates filopodia formation at the branch tips through unknown effectors (Ribeiro et al., 2002). How these filopodia contribute to migration was hampered by the fact that, in *btl* mutants, filopodia were not formed and, in addition, tip cells were not properly specified. In this study we identify *sn* as a target of Btl activity. In *sn* mutants, filopodia form but they are defective, allowing us to assess their relevance in branching and migration. Furthermore, our results unveil a dual regulation of filopodia by the Btl pathway, as it is both required for filopodia formation in a transcriptional-independent manner (Ribeiro et al., 2002) and for filopodia organisation in a transcriptional-dependent (Pnt-mediated) manner (this study).

Sn is specifically upregulated in branch tip cells in response to Btl activation. Similarly, Fascins are expressed in epithelial cells that require specific programmes for motility or epithelial to mesenchymal progression (Machesky and Li, 2010). The restricted expression of

Development (2014) doi:10.1242/dev.103218

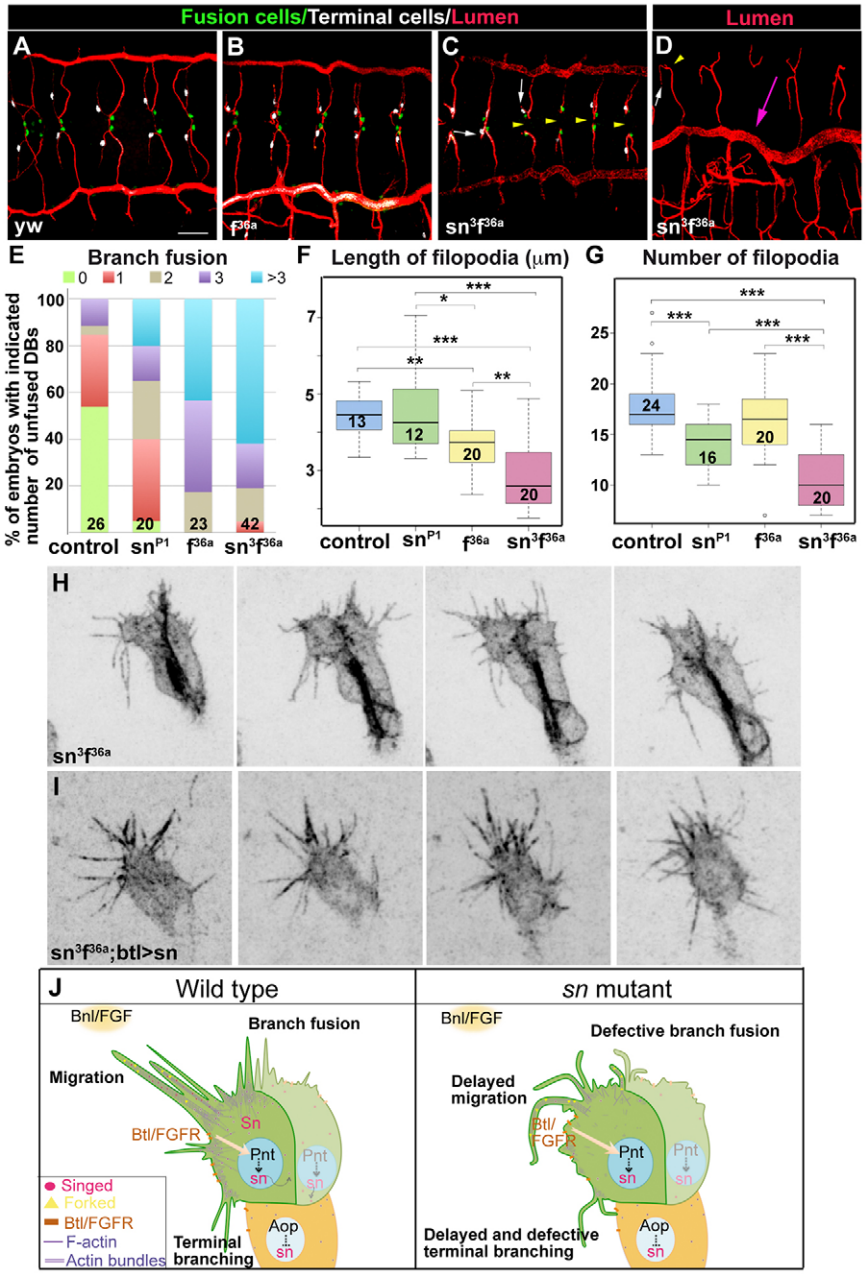

Fig. 7. Interactions of *sn* and *f* in tracheal formation. (A-D) Stage 16 embryos marked by 2A12 (red), Dys (green) and Dsrf (white). Note the defects in double mutants in branch fusion (yellow arrowheads), terminal branching (white arrows) and DB formation (pink arrow). (E) Penetrance and expressivity of fusion. Colours indicate the number of defects per embryo. (F,G) Quantification of number and length of filopodia of terminal cells. Note the strong defects in double mutants. Numbers inside boxes correspond to number of terminal cells analysed. (H,I) Time-lapse images of DB tip cells at stage 15. Note the short and rudimentary filopodia and irregular cell shape in double mutants (H) and the rescue when *sn* is overexpressed (I). (J) *sn* is upregulated in tip cells upon Btl activation. *sn* (in concert with *f*) regulates actin-based filopodia and cytoplasmic extensions. Sn provides stiffness to filopodia and contributes to the organisation of advancing cell fronts. In the absence of Sn, actin-based structures are not properly organised to ensure timely and directed migration, branch fusion and terminal branching. Scale bar: 25 μm.

fascins is physiologically relevant because their misregulation can cause severe disorders. For instance, fascin-1 misexpression is observed in several carcinomas and correlates with a poor prognosis (Hashimoto et al., 2011; Machesky and Li, 2010). Fascin-1 stabilises actin bundles in invadopodia (Li et al., 2010), which are long filopodia-like protrusions in cancer cells thought to stimulate invasion and cancer metastasis (Sibony-Benyamini and Gil-Henn, 2012; Yamaguchi, 2012). But in spite of the importance of fascins both in physiological and pathological conditions, only a few regulatory transcriptional mechanisms have been described so far (Hashimoto et al., 2011). Therefore, identifying fascin regulators, as we do in this study, is relevant for the biomedical field. We suggest that the Btl pathway, acting through its canonical pathway, might be a general regulator of *sn* in migrating cells. Importantly, dysregulation of FGF signalling has also been observed in tumour formation and progression (Brooks et al., 2012), suggesting that dysregulation of fascin could mediate in part this malignant FGFR activity.

sn regulation of filopodia stiffness and tip cell shape controls tracheal tissue morphogenesis

We identified two types of defects in *sn* mutants at the cellular level: filopodia defects and cell shape defects. Filopodia defects were penetrant and consisted of curved and apparently flaccid filopodia that often orient parallel to the membrane, in contrast to the straight, stiff and perpendicular filopodia of control embryos. We propose that these defects are due to the abnormal actin organisation we describe: whereas in the wild type long and conspicuous actin ribs are detected and actin clearly accumulates at the filopodia base, in *sn* mutants only punctae or short bundles are detected in the lamellae and no clear actin accumulation is observed at the base of filopodia. Thus, our results are consistent with the described activity of *sn*, cross-linking actin filaments into bundles that provide stiffness to filopodia (Hashimoto et al., 2011; Vignjevic et al., 2006; Vignjevic and Montagnac, 2008). Besides filopodia, *sn* is required in other types of actin-based structures in flies, such as actin bundles in nurse

Development (2014) doi:10.1242/dev.103218

cells (Cant et al., 1994), dendrite terminal branchlets in sensory neurons (Nagel et al., 2012), actin bundles in the bristles (Cant et al., 1994; Overton, 1967; Tilney et al., 1995) or lamellae microspikes in plasmatocytes (Zanet et al., 2009). In these structures *sn* promotes the formation of straight and stiff structures, whereas its absence leads to the formation of curved ones.

Besides filopodia defects, the morphology of tracheal tip cells was clearly irregular in *sn* mutants and the cytoplasmic processes of terminal and fusion cells were often delayed or abnormal. These cell shape defects may derive from the defective filopodia, which would be inefficient to deform the membrane or stabilise this deformation. Additionally, we propose that they also reflect a role for the *sn*-dependent microspikes and cortical actin meshwork at the lamellipodia that we describe, which would be able to generate membrane protrusions that shape the tip cells. The *sn*-dependent actin accumulation at the lamellipodia and its role in tracheal cell shape is consistent with evidence in other cell types showing that fascin forms densely packed, parallel actin bundles that provide rigidity to push out membrane tethers upon protrusion (Schäfer et al., 2011), as in vertebrate and *Drosophila* lamellipodia (Adams, 1997; Nemethova et al., 2008; Zanet et al., 2009) or in invadopodia (Li et al., 2010; Schoumacher et al., 2010).

Are these defects at the cellular level underlying the tracheal tissue defects in *sn* mutants? We propose that they are and that the defects in tracheal formation stem from the defective filopodia and cell morphologies (Fig. 7J). In the case of branch extension, we propose that the abnormal filopodia and lamellipodia of *sn* mutants are not sufficient to support the *bnl*-mediated migration, producing branch growth delays. This is in agreement with reported evidences indicating that cell migration requires filopodia to sense the environment and to adhere to the substrate to transmit the force to advance (Adams, 2004; Schäfer et al., 2011) and that lamellipodia are a crucial protrusive component of migrating cells. In the case of branch fusion and terminal branch extension defects, we propose that they are due to the defective advance of lamellipodia, which impair a timely and efficient branching and fusion, or to defective exploratory-recognition abilities of filopodia in branch fusion. Finally, in the case of terminal lumen guidance, it was shown that it requires an actin network that directs lumen pathfinding (Oshima et al., 2006). Our results provide new insights into this mechanism by showing that this actin network needs to be properly bundled.

Strikingly, we also find a role for *sn* in regulating tracheal cell specification, as we observed presence of extra terminal cells expressing Dsrf in *sn* mutant conditions. Previous reports may shed light into the possible mechanism of this phenotype, as it was described that actin dynamics can regulate Dsrf activity, which can regulate its own expression (Miralles et al., 2003; Somogyi and Rørth, 2004; Sotiropoulos et al., 1999). Alternatively, the misregulation of Dsrf expression may be indirectly caused by an abnormal branch extension producing altered reception of cell specification signals or altered tip cell interactions.

Molecular requirements for *sn* during tracheal formation

Our current knowledge of fascins unveils an enormous complexity. Fascins act as actin-bundling proteins (Khurana and George, 2011) and this activity is regulated by phosphorylation on S52 in flies/S39 in vertebrates (Tilney et al., 2000; Vignjevic et al., 2006; Yamakita et al., 1996; Zanet et al., 2009). However, in *in vivo* systems such as *Drosophila*, phosphorylation on S52 inactivates *sn* activity in certain conditions but not in others (Zanet et al., 2009). Furthermore, although it is widely accepted that fascins act as actin-bundling proteins, a recent report proposed a bundling-independent activity of fascins that promote filopodia formation (Zanet et al., 2012).

Our work in an *in vivo* system sheds light into *sn* and actin-based mechanisms. Our results are consistent with a requirement of the actin-bundling activity of *sn*, regulated by phosphorylation on S52, for proper tracheal formation. This conclusion is based on the observation that the phosphomimetic form Sn^{S52E} cannot rescue *sn* tracheal defects, whereas the non-phosphorylatable form Sn^{S52A}, as well as wild-type Sn, rescue these defects. This correlates with the subcellular accumulation of these phosphovariants: Sn^{S52A} is clearly enriched in filopodia protrusions whereas Sn^{S52E} accumulation is more cytoplasmic. Our results are in line with results in bristles (Zanet et al., 2009) and sensory neurons (Nagel et al., 2012) but in contrast with observations in plasmatocytes and nurse cells (Zanet et al., 2009). Remarkably, we find that Sn regulation in plasmatocytes and tracheal cells is different not only at the post-transcriptional level, but also at the transcriptional one; although Btl regulates *sn* expression in the tracheal tissue, it does not regulate it in plasmatocytes. Altogether this indicates that *sn* can employ different molecular mechanisms that are cell-type and context specific.

The parallels for *sn* during tracheal and bristle formation extend beyond the requirement of *sn*-bundling activity, as in both cell types *f* interacts with *sn*. In bristles, F and Sn bind and act sequentially to cross-link actin filaments [reviewed by Tilney and DeRosier (Tilney and DeRosier, 2005)]. F appears at early stages of bristle formation and organises previously formed (by an unidentified cross-linker) actin bundlets into loosely ordered modules. Sn appears later, displacing F and tightly organising the bundles into hexagonally packed structures, thereby increasing rigidity. Hence, in the absence of *f* the number of actin filaments per bundle are decreased but they are regularly packed, in the absence of *sn* more actin filaments per bundle are present but these are not hexagonally packed, and in the absence of both almost no actin filaments arrange into bundles (Tilney et al., 2003; Tilney et al., 1995). We find that a similar mechanism may be operating in tracheal filopodia: whereas absence of each cross-linker affects filopodia morphology, length (*f* mutants) or number (*sn* mutants), the absence of both proteins strongly affects all features. Thus, our results show, for the first time, a role for F in transient actin structures, as it is the case in tracheal filopodia. Furthermore, our experiments provide new insights into the mechanisms of actin bundling. While we show that F and Sn provide distinct functions to filopodia organisation indicating that in normal conditions both cross-linkers are required, our rescue experiments also indicate that Sn can overcome F requirements and restore filopodia organisation in overexpression conditions, indicating that their activities are partially redundant.

Intriguingly, in *fsn* mutants many terminal cells are not differentiated. Terminal cell specification requires Btl signal (Guillemin et al., 1996; Samakovlis et al., 1996a). The fact that in *fsn* double mutants there are few and short filopodia and that the cell fronts are incorrectly organised, leads us to speculate that Bnl signal might not be properly received by tracheal tip cells. Indeed, besides the recognised role of filopodia in environment sensing acting as mechanosensitive organelles, filopodia are also proposed to play roles in responding to external guiding cues, here acting as chemosensitive organelles (Khurana and George, 2011).

MATERIALS AND METHODS

Genetics

y^1w^{1118} (wild type), sn^{P1}, sn^{28}, f^{36a}, sn^3f^{36a}, bnl^{00857} (bnl^{P1}), $pnt^{\Delta 88}$ and aop^2 (aop^{11S}) are described in FlyBase. *ETS-12* (*lacZ* line) revealed *pnt*

expression. Mutant chromosome were balanced over marked balancers. For overexpression in the trachea we used *btlGal4*. The transgenes used are described in FlyBase: *UAS-GFPsn*, *UAS-GFPsn*^{S52E}, *UAS-GFPsn*^{S52A} (kindly provided by S. Plaza), *UAS-bnl*, *btl-MoeGFP*, *UAS-pnt*, *UAS-aop*$^{act.2}$, *UAS-UtrGFP* (kindly provided by T. Lecuit) and *UAS-snRNAi* (from VDRC and Bloomington Stock Center). In panels labelled 'tracheal cells' the embryos were stained for Trachealess (Trh, nuclear staining) or for GFP in embryos carrying *btlGal4 UAS-srcGFP* (cell membrane staining).

Immunohistochemistry and *in situ* hybridisation

We followed standard protocols for immunostainings and *in situ* hybridisations. The following primary antibodies were used: mouse anti-Sn [Developmental Studies Hybridoma Bank (DSHB)], mouse mAb2A12 (to visualise the tracheal lumen; DSHB), mouse anti-mActin (MP Biomedicals), rat anti-Trh (J. Casanova's lab), rabbit or goat anti-GFP (Molecular Probes and Roche), chicken anti-β-gal (Abcam), rabbit anti-Dys and mouse anti-Dsrf.

An *f* riboprobe was generated using the following primers: forward, 5′-AGATACAGATCGCCCAGCAG-3′; reverse, 5′-TGTGATTTGCCAGACA-TGGT-3′.

Image acquisition and analysis of fixed embryos

Confocal images of fixed embryos were obtained with a Leica TCS-SPE system. Images were imported into Fiji and Photoshop, and assembled using Illustrator.

The Fiji Freehand Line tool was used to measure the length of the terminal cell filopodia of fixed stage 16 embryos carrying *btlGal4-UASsrcGFP* in the indicated backgrounds.

Quantifications and statistics

Total number of embryos, DBs or terminal cells (n) are provided in text and figures. Error bars indicate standard error (s.e.). *P*-values were obtained with two-sample *t*-test using R Commander v1.7-0 software (http://cran.r-project.org/bin/macosx/) or with Fisher's exact test (http://www.langsrud.com/fisher.htm#INTRO) for binomial distributions. **P*<0.05, ***P*<0.01, ****P*<0.001.

Time-lapse imaging

Live imaging was performed on an inverted Leica TCS-SP5 or a Zeiss Lsm780 confocal. Dechorionated embryos were mounted on Menzel-Gläser coverslips with glue and covered with Oil 10-S Voltalef (VWR).

To measure DB approaching, GFP fluorescence was captured every 90 seconds over 26-58 µm *z*-stacks of stage 13-14 embryos mounted dorsally and recorded in a Leica TCS-SP5 during ~3 hours. Each DB front was manually followed with the Fiji Manual Tracking, and the results were treated in Excel.

To follow tip cell filopodia and cell shape changes we visualised stage 14-15 *btlGal4-UASsrcGFP* embryos in the indicated genetic backgrounds. Embryos were imaged in a Leica TCS-SP5 at 10-second intervals with 16×0.67-0.86 µm *z*-stacks.

To analyse actin dynamics we used *btlGal4-UASUtrGFP* or *btl-MoeGFP* in different genetic backgrounds and acquired images of 0.82-0.85 µm *z*-stacks every 14 seconds in a Zeiss Lsm780 using a water 63× objective and 1.8 zoom.

To measure the correlation of the angle of dorsoanterior filopodia with respect to branch migration, we measured all dorsoanterior filopodial angles of tip cells of stage 14 control embryos (*btlGal4-UASsrcGFP*) every minute using the Straight Line Selection tool of Fiji software. We compared the average of these angles with the tip cell advance. Tip cell advance was estimated with the Manual Tracking tool of Fiji software by following a path obtained by analysing every minute the position of the terminal cell front (measured at three different positions in the front).

To compare the straightness of filopodia between stage 14 control (*btlGal4-UASsrcGFP*) and *sn* mutants (*sn*^{P1}*; btlGal4-UASsrcGFP*) we measured the number of new bent filopodia (with an angle higher than 135°) formed and normalized it with the number of filopodia at each time point.

Tiff original supplementary material movies are shown as Avi and compressed as PNG.

Measurements were imported and treated into Excel software, and R Commander software was used for statistics.

Acknowledgements

We thank N. Luque, E. Fuentes, E. Rebollo and L. Bardia for technical assistance. We are grateful to S. Plaza and J. Zanet for reagents and the Developmental Studies Hybridoma Bank, the Bloomington Stock Center and Vienna Drosophila RNAi Centre for fly lines and antibodies. We thank members of the Llimargas and Casanova labs for helpful discussions and J. Casanova, M. Furriols, A. Letizia, S. Araújo, S. Ricardo and G. Lebréton for critically reading the manuscript.

Competing interests

The authors declare no competing financial interests.

Author contributions

P.O.-R. and M.L. designed the research and interpreted the results. P.O.-R. performed experiments and quantifications and M.L. wrote the paper.

Funding

P.O.-R. is supported by a FPI fellowship from Ministerio de Ciencia e Innovación. This work was supported by funds from the Ministerio de Ciencia e Innovación to M.L. [BFU2006-09515/BMC, BFU2009-09041] and from Programme Consolider 2007 [CSD2007-00008] project.

Supplementary material

Supplementary material available online at
http://dev.biologists.org/lookup/suppl/doi:10.1242/dev.103218/-/DC1

References

Adams, J. C. (1997). Characterization of cell-matrix adhesion requirements for the formation of fascin microspikes. *Mol. Biol. Cell* **8**, 2345-2363.
Adams, J. C. (2004). Roles of fascin in cell adhesion and motility. *Curr. Opin. Cell Biol.* **16**, 590-596.
Affolter, M., Bellusci, S., Itoh, N., Shilo, B., Thiery, J. P. and Werb, Z. (2003). Tube or not tube: remodeling epithelial tissues by branching morphogenesis. *Dev. Cell* **4**, 11-18.
Bartles, J. R., Wierda, A. and Zheng, L. (1996). Identification and characterization of espin, an actin-binding protein localized to the F-actin-rich junctional plaques of Sertoli cell ectoplasmic specializations. *J. Cell Sci.* **109**, 1229-1239.
Brooks, A. N., Kilgour, E. and Smith, P. D. (2012). Molecular pathways: fibroblast growth factor signaling: a new therapeutic opportunity in cancer. *Clin. Cancer Res.* **18**, 1855-1862.
Cabernard, C. and Affolter, M. (2005). Distinct roles for two receptor tyrosine kinases in epithelial branching morphogenesis in Drosophila. *Dev. Cell* **9**, 831-842.
Cant, K., Knowles, B. A., Mooseker, M. S. and Cooley, L. (1994). Drosophila singed, a fascin homolog, is required for actin bundle formation during oogenesis and bristle extension. *J. Cell Biol.* **125**, 369-380.
Cant, K., Knowles, B. A., Mahajan-Miklos, S., Heintzelman, M. and Cooley, L. (1998). Drosophila fascin mutants are rescued by overexpression of the villin-like protein, quail. *J. Cell Sci.* **111**, 213-221.
Faix, J., Breitsprecher, D., Stradal, T. E. and Rottner, K. (2009). Filopodia: complex models for simple rods. *Int. J. Biochem. Cell Biol.* **41**, 1656-1664.
Gervais, L. and Casanova, J. (2010). In vivo coupling of cell elongation and lumen formation in a single cell. *Curr. Biol.* **20**, 359-366.
Gervais, L., Lebreton, G. and Casanova, J. (2012). The making of a fusion branch in the Drosophila trachea. *Dev. Biol.* **362**, 187-193.
Ghabrial, A., Luschnig, S., Metzstein, M. M. and Krasnow, M. A. (2003). Branching morphogenesis of the Drosophila tracheal system. *Annu. Rev. Cell Dev. Biol.* **19**, 623-647.
Guillemin, K., Groppe, J., Ducker, K., Treisman, R., Hafen, E., Affolter, M. and Krasnow, M. A. (1996). The pruned gene encodes the Drosophila serum response factor and regulates cytoplasmic outgrowth during terminal branching of the tracheal system. *Development* **122**, 1353-1362.
Hashimoto, Y., Kim, D. J. and Adams, J. C. (2011). The roles of fascins in health and disease. *J. Pathol.* **224**, 289-300.
Hogan, B. L. and Kolodziej, P. A. (2002). Organogenesis: molecular mechanisms of tubulogenesis. *Nat. Rev. Genet.* **3**, 513-523.
Jiang, L. and Crews, S. T. (2003). The Drosophila dysfusion basic helix-loop-helix (bHLH)-PAS gene controls tracheal fusion and levels of the trachealess bHLH-PAS protein. *Mol. Cell. Biol.* **23**, 5625-5637.
Kato, K., Chihara, T. and Hayashi, S. (2004). Hedgehog and Decapentaplegic instruct polarized growth of cell extensions in the Drosophila trachea. *Development* **131**, 5253-5261.
Khurana, S. and George, S. P. (2011). The role of actin bundling proteins in the assembly of filopodia in epithelial cells. *Cell Adh. Migr.* **5**, 409-420.
Klämbt, C., Glazer, L. and Shilo, B. Z. (1992). breathless, a Drosophila FGF receptor homolog, is essential for migration of tracheal and specific midline glial cells. *Genes Dev.* **6**, 1668-1678.
Lee, S. and Kolodziej, P. A. (2002). The plakin Short Stop and the RhoA GTPase are required for E-cadherin-dependent apical surface remodeling during tracheal tube fusion. *Development* **129**, 1509-1520.

Lee, M., Lee, S., Zadeh, A. D. and Kolodziej, P. A. (2003). Distinct sites in E-cadherin regulate different steps in Drosophila tracheal tube fusion. *Development* **130**, 5989-5999.
Li, A., Dawson, J. C., Forero-Vargas, M., Spence, H. J., Yu, X., König, I., Anderson, K. and Machesky, L. M. (2010). The actin-bundling protein fascin stabilizes actin in invadopodia and potentiates protrusive invasion. *Curr. Biol.* **20**, 339-345.
Lubarsky, B. and Krasnow, M. A. (2003). Tube morphogenesis: making and shaping biological tubes. *Cell* **112**, 19-28.
Machesky, L. M. and Li, A. (2010). Fascin: Invasive filopodia promoting metastasis. *Commun. Integr. Biol.* **3**, 263-270.
Miralles, F., Posern, G., Zaromytidou, A. I. and Treisman, R. (2003). Actin dynamics control SRF activity by regulation of its coactivator MAL. *Cell* **113**, 329-342.
Nagel, J., Delandre, C., Zhang, Y., Förstner, F., Moore, A. W. and Tavosanis, G. (2012). Fascin controls neuronal class-specific dendrite arbor morphology. *Development* **139**, 2999-3009.
Nemethova, M., Auinger, S. and Small, J. V. (2008). Building the actin cytoskeleton: filopodia contribute to the construction of contractile bundles in the lamella. *J. Cell Biol.* **180**, 1233-1244.
Ohshiro, T., Emori, Y. and Saigo, K. (2002). Ligand-dependent activation of breathless FGF receptor gene in Drosophila developing trachea. *Mech. Dev.* **114**, 3-11.
Oshima, K., Takeda, M., Kuranaga, E., Ueda, R., Aigaki, T., Miura, M. and Hayashi, S. (2006). IKK epsilon regulates F actin assembly and interacts with Drosophila IAP1 in cellular morphogenesis. *Curr. Biol.* **16**, 1531-1537.
Overton, J. (1967). The fine structure of developing bristles in wild type and mutant Drosophila melanogaster. *J. Morphol.* **122**, 367-379.
Ribeiro, C., Ebner, A. and Affolter, M. (2002). In vivo imaging reveals different cellular functions for FGF and Dpp signaling in tracheal branching morphogenesis. *Dev. Cell* **2**, 677-683.
Samakovlis, C., Hacohen, N., Manning, G., Sutherland, D. C., Guillemin, K. and Krasnow, M. A. (1996a). Development of the Drosophila tracheal system occurs by a series of morphologically distinct but genetically coupled branching events. *Development* **122**, 1395-1407.
Samakovlis, C., Manning, G., Steneberg, P., Hacohen, N., Cantera, R. and Krasnow, M. A. (1996b). Genetic control of epithelial tube fusion during Drosophila tracheal development. *Development* **122**, 3531-3536.
Schäfer, C., Faust, U., Kirchgessner, N., Merkel, R. and Hoffmann, B. (2011). The filopodium: a stable structure with highly regulated repetitive cycles of elongation and persistence depending on the actin cross-linker fascin. *Cell Adh. Migr.* **5**, 431-438.
Schoumacher, M., Goldman, R. D., Louvard, D. and Vignjevic, D. M. (2010). Actin, microtubules, and vimentin intermediate filaments cooperate for elongation of invadopodia. *J. Cell Biol.* **189**, 541-556.
Sibony-Benyamini, H. and Gil-Henn, H. (2012). Invadopodia: the leading force. *Eur. J. Cell Biol.* **91**, 896-901.
Somogyi, K. and Rørth, P. (2004). Evidence for tension-based regulation of Drosophila MAL and SRF during invasive cell migration. *Dev. Cell* **7**, 85-93.
Sotiropoulos, A., Gineitis, D., Copeland, J. and Treisman, R. (1999). Signal-regulated activation of serum response factor is mediated by changes in actin dynamics. *Cell* **98**, 159-169.
Sutherland, D., Samakovlis, C. and Krasnow, M. A. (1996). branchless encodes a Drosophila FGF homolog that controls tracheal cell migration and the pattern of branching. *Cell* **87**, 1091-1101.
Tanaka-Matakatsu, M., Uemura, T., Oda, H., Takeichi, M. and Hayashi, S. (1996). Cadherin-mediated cell adhesion and cell motility in Drosophila trachea regulated by the transcription factor Escargot. *Development* **122**, 3697-3705.
Tilney, L. G. and DeRosier, D. J. (2005). How to make a curved Drosophila bristle using straight actin bundles. *Proc. Natl. Acad. Sci. USA* **102**, 18785-18792.
Tilney, L. G., Tilney, M. S. and Guild, G. M. (1995). F actin bundles in Drosophila bristles. I. Two filament cross-links are involved in bundling. *J. Cell Biol.* **130**, 629-638.
Tilney, L. G., Connelly, P. S., Vranich, K. A., Shaw, M. K. and Guild, G. M. (1998). Why are two different cross-linkers necessary for actin bundle formation in vivo and what does each cross-link contribute? *J. Cell Biol.* **143**, 121-133.
Tilney, L. G., Connelly, P. S., Vranich, K. A., Shaw, M. K. and Guild, G. M. (2000). Regulation of actin filament cross-linking and bundle shape in Drosophila bristles. *J. Cell Biol.* **148**, 87-100.
Tilney, L. G., Connelly, P. S., Ruggiero, L., Vranich, K. A. and Guild, G. M. (2003). Actin filament turnover regulated by cross-linking accounts for the size, shape, location, and number of actin bundles in Drosophila bristles. *Mol. Biol. Cell* **14**, 3953-3966.
Vignjevic, D. and Montagnac, G. (2008). Reorganisation of the dendritic actin network during cancer cell migration and invasion. *Semin. Cancer Biol.* **18**, 12-22.
Vignjevic, D., Kojima, S., Aratyn, Y., Danciu, O., Svitkina, T. and Borisy, G. G. (2006). Role of fascin in filopodial protrusion. *J. Cell Biol.* **174**, 863-875.
Yamaguchi, H. (2012). Pathological roles of invadopodia in cancer invasion and metastasis. *Eur. J. Cell Biol.* **91**, 902-907.
Yamakita, Y., Ono, S., Matsumura, F. and Yamashiro, S. (1996). Phosphorylation of human fascin inhibits its actin binding and bundling activities. *J. Biol. Chem.* **271**, 12632-12638.
Yang, S., Huang, F. K., Huang, J., Chen, S., Jakoncic, J., Leo-Macias, A., Diaz-Avalos, R., Chen, L., Zhang, J. J. and Huang, X. Y. (2013). Molecular mechanism of fascin function in filopodial formation. *J. Biol. Chem.* **288**, 274-284.
Zanet, J., Stramer, B., Millard, T., Martin, P., Payre, F. and Plaza, S. (2009). Fascin is required for blood cell migration during Drosophila embryogenesis. *Development* **136**, 2557-2565.
Zanet, J., Jayo, A., Plaza, S., Millard, T., Parsons, M. and Stramer, B. (2012). Fascin promotes filopodia formation independent of its role in actin bundling. *J. Cell Biol.* **197**, 477-486.

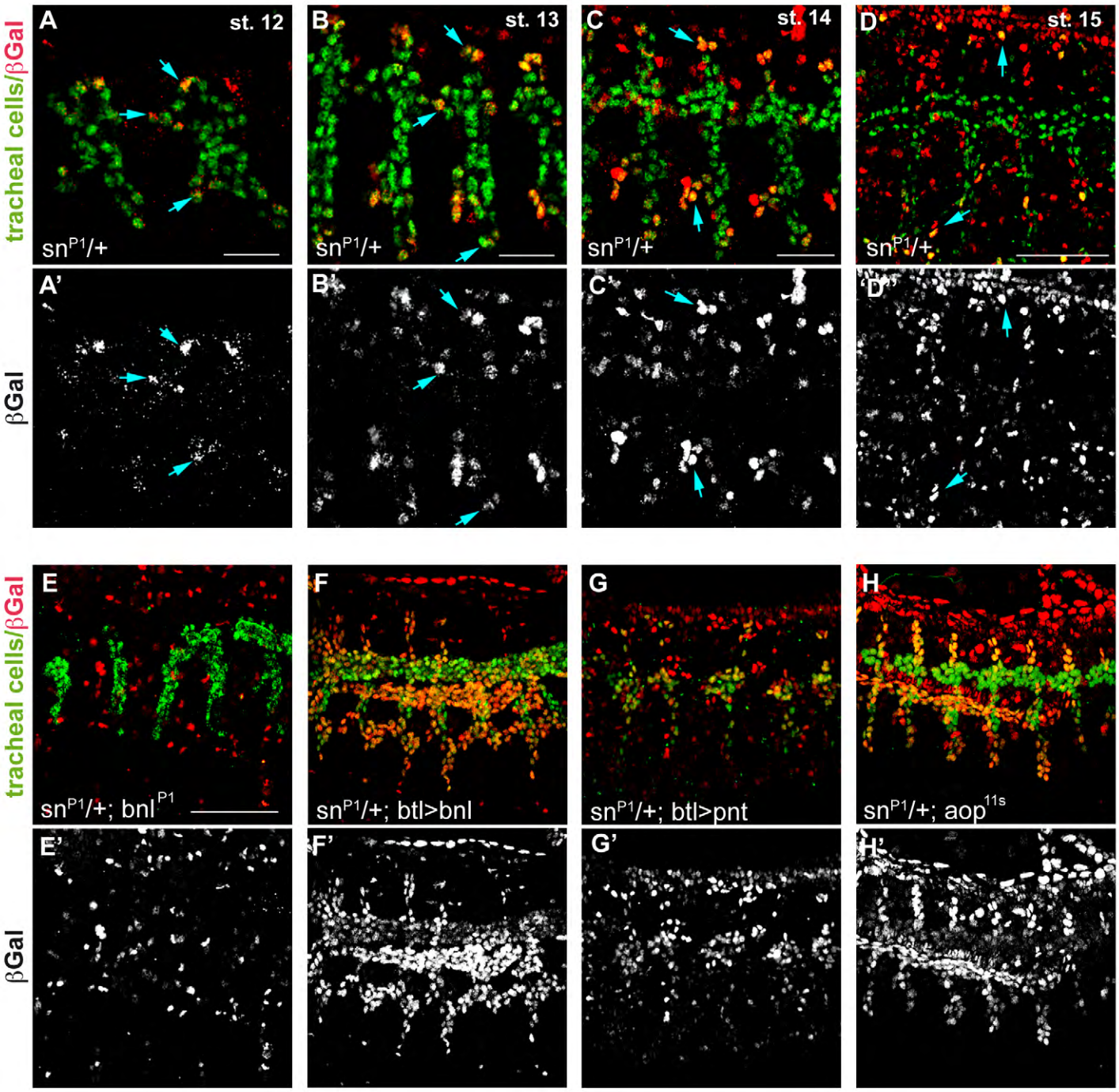

Figure S1: Expression of *sn* and its regulation during tracheal development

Embryos showing tracheal cells (green) and *sn* transcriptional pattern (red or white) visualised using a *sn-lacZ* line in heterozgous conditions (sn^{P1}). (A-D) Embryos at indicated stages showing *sn* expression. Note the expression at the tip of the branches (blue arrows). (E-H) Pattern of *sn* expression in embryos at stages 14-15 in the genetic backgrounds indicated. Note the absence of *sn* expression in *bnl* mutants and the generalised expression when *bnl* or *pnt* are overexpressed or in *aop* mutants.

Scale bar A,B,C 10 μm; D,E 25 μm.

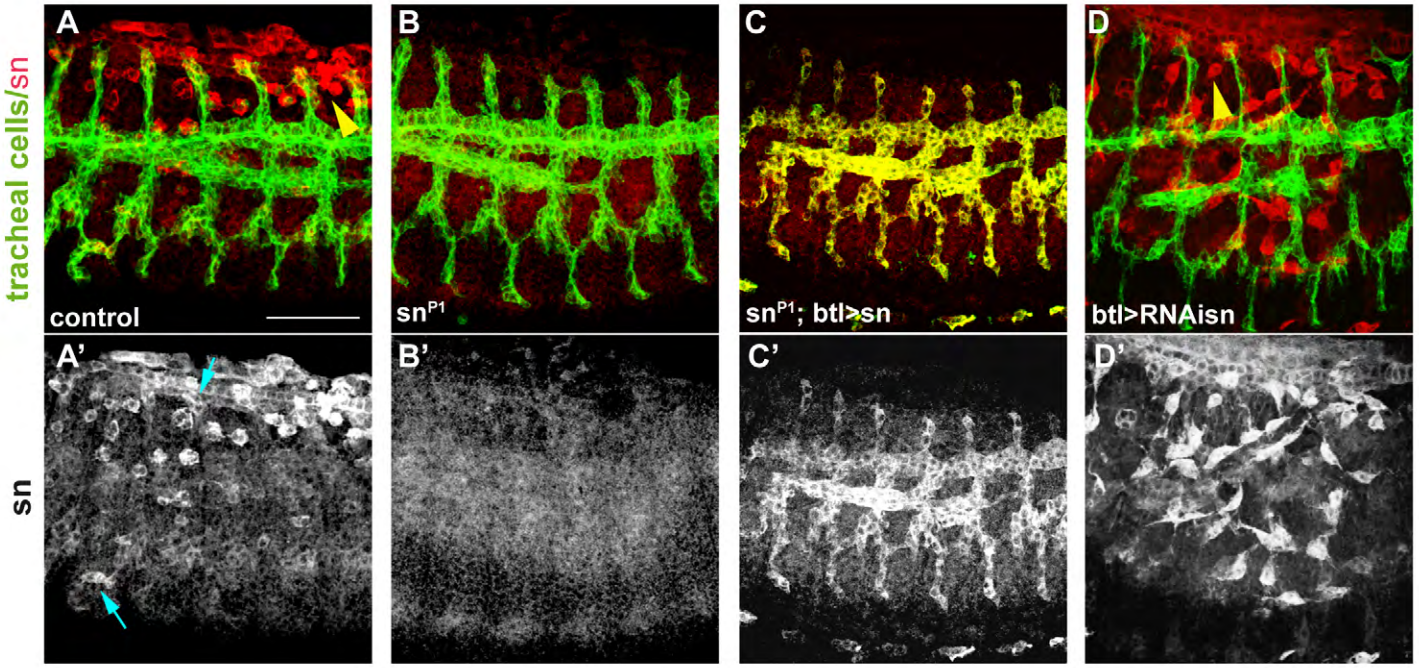

Figure S2: Pattern of Sn accumulation in *sn* mutant conditions

Stage 14-15 embryos carrying *btlGal4>UASsrcGFP* stained for tracheal cells (green) and Sn protein accumulation (red or white) in the genetic backgrounds indicated. Blue arrows point to tracheal tip cells and yellow arrowheads point to plasmatocytes.

Scale bar 25 μm.

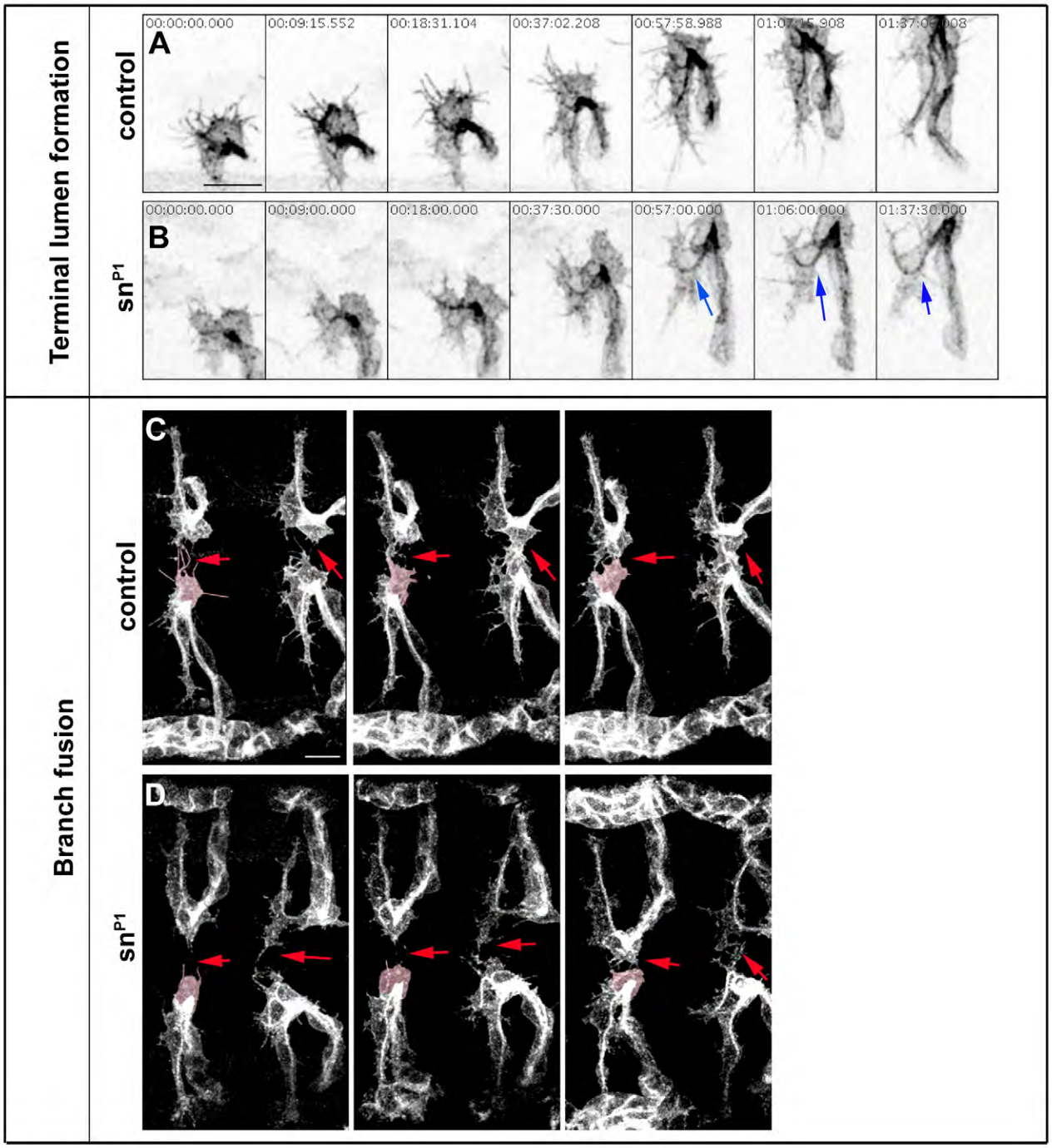

Figure S3: Fusion and terminal branching defects in *sn* mutants

(A,B) Images of time-lapse movies of control and *sn* mutants marked with *btl>srcGFP* showing a lumen missguidance in the mutant (blue arrows), which elongates dorsally instead of ventrally.

(C,D) Images of time-lapse movies of control and *sn* mutants marked with *btl>srcGFP* showing two pairs of contralateral DBs during branch fusion (red arrows). The shape of one of the fusion cells is highlighted. Note the abnormal filopodia contact and cell front advance in *sn* mutant fusion cells (D) as compared to wild type (C).

Scale bar 10 μm

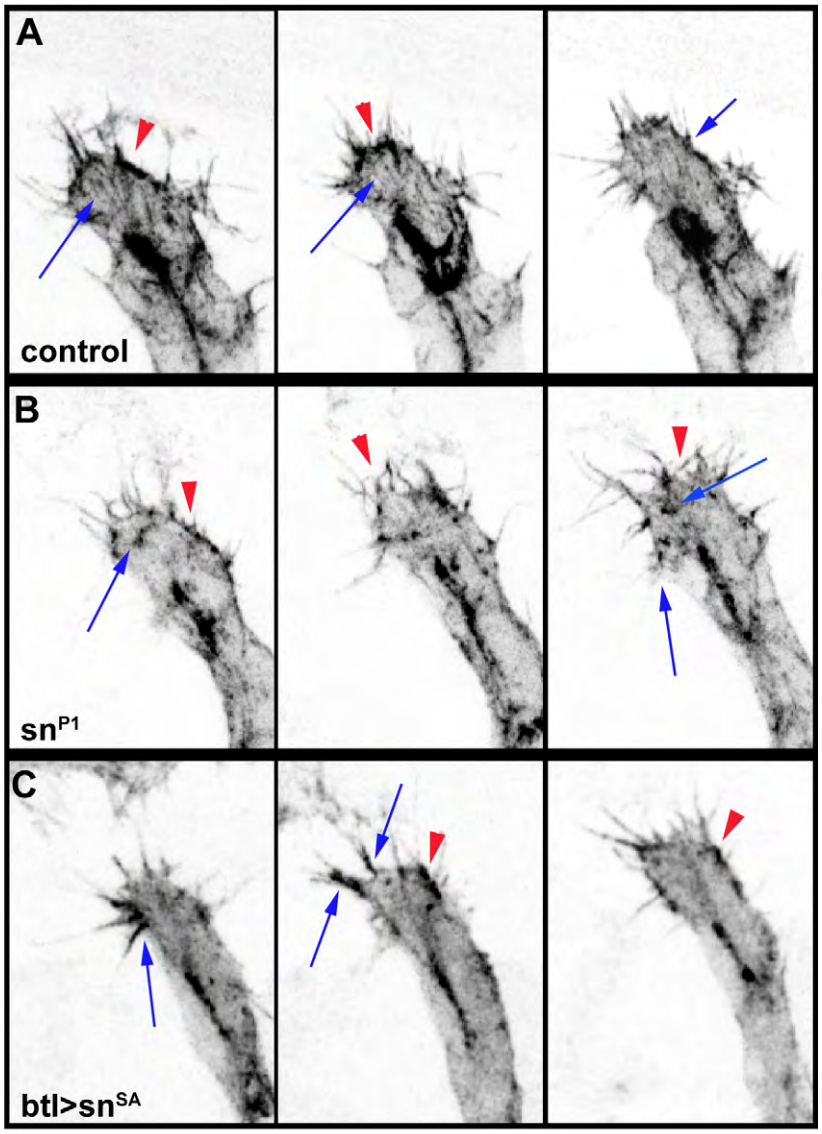

Figure S4: *sn* is required for proper actin organisation

Images from time-lapse movies of embryos with *btl>moeGFP* showing actin organisation. In *sn* mutants (B) the actin accumulation at the lamellipodia (red arrowhead) and filopodia (blue arrows) is less conspicuous as compared to the wild type (A). Note the abnormal accumulation of actin in punctae or short bundles in the mutants (blue arrows). In sn^{SA} conditions (C) high accumulation of actin can be detected along the filopodia, while in the wild-type filopodia actin accumulates at their base (A).

Scale bar 5 μm

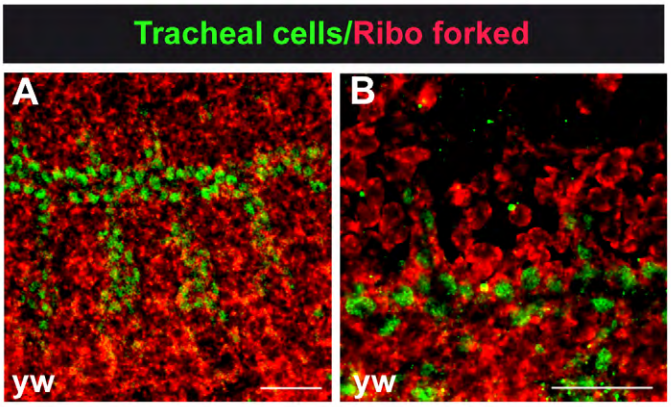

Figure S5: *f* expression
Whole mount in situ hybridisation showing the presence of *f* transcript in tracheal cells (green).
Scale bar A 25 µm; B 10 µm

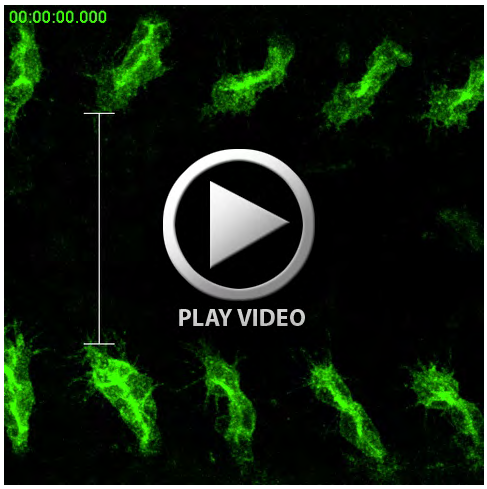

Movie 1 (Figure 3D,D'): Approaching of dorsal branches during tracheal development
Embryo carrying *btlGal4>UASsrcGFP* visualised from a dorsal view using an inverted TCS-SP5 confocal microscope with a 63.0x1.40 Oil objective. Time-lapse images were taken every 1min30sec. Distance between contralateral DB4 is marked by a bar and the fusion point by an astersik at time point 0, 1 hour and 1 hour 25 min (indicated by an arrowhead).

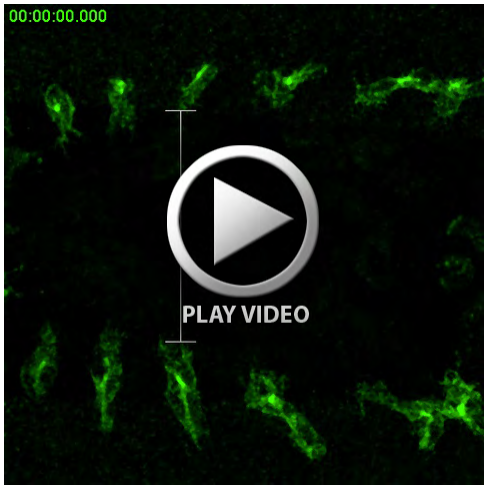

Movie 2 (Figure 3E,E'): Delayed approaching of dorsal branches in *sn* mutant
Embryo mutant for *sn* (sn^{P1}) and carrying *btlGal4>UASsrcGFP* visualised from a dorsal view using an inverted TCS-SP5 confocal microscope with a 63.0x1.40 Oil objective. Time-lapse images were taken every 1min30sec. Distance between contralateral DB4 is marked at time point 0, 1 hour and 1 hour 25 min (indicated by an arrowhead). Note that DB4 is several minutes delayed to cover the same distance (indicated by bars or asterisk) when compared to control embryos (Movie 1). Yellow arrow points to a DB missguidance.

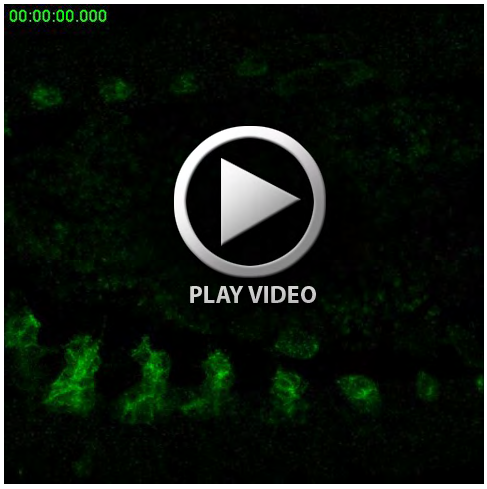

Movie 3: Branch outgrowth, branch fusion and terminal branching in control dorsal branches

Embryo carrying *btlGal4>UASsrcGFP* visualised from a lateral view using an inverted TCS-SP5 confocal microscope with a 63.0x1.40 Oil objective. Time-lapse images were taken every 1min14sec and 1min59sec and concatenated post-imaging. Note the formation of the cytoplasmic extension of terminal cells starting before dorsal branch fusion (white arrows). Branch fusion at the dorsal midline is marked by white asterisks.

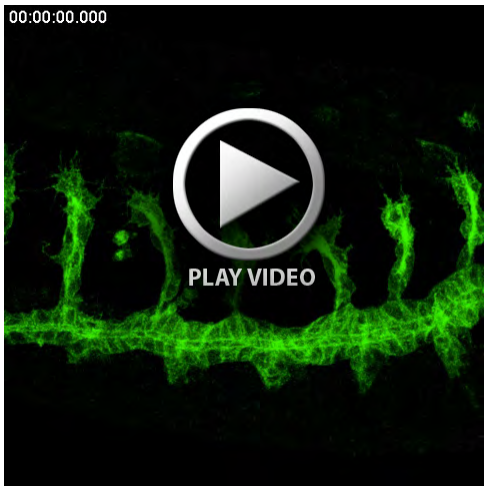

Movie 4: Defective branch outgrowth, branch fusion and terminal branching in *sn* mutants

Embryo mutant for *sn* (sn^{P1}) and carrying *btlGal4>UASsrcGFP* visualised from a lateral view using an inverted TCS-SP5 confocal microscope with a 63.0x1.40 Oil objective. Time-lapse images were taken every 2min7sec. Note that cytoplasmic extensions are delayed (white arrows) when compared to the control embryos (Movie3). Several dorsal branches remain unfused at the end of embryogenesis (red asterisks). Note the formation of a misguided terminal lumen (yellow arrowhead) that turns dorsally.

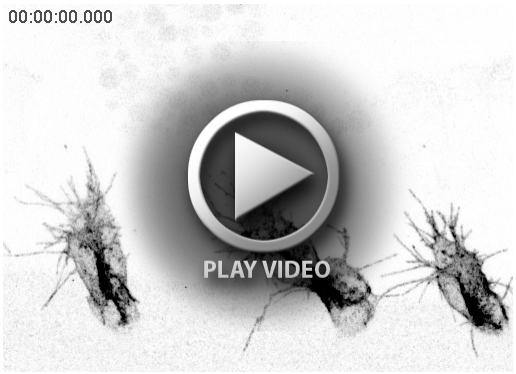

Movie 5 (Figure 5A): Fast time-lapse imaging of filopodia and tip-cell shape in control dorsal branches

Live imaging of DB tip cells of control embryo (*btlGal4>UASsrcGFP*) was acquired using an inverted TCS-SP5 confocal microscope with a 63.0x1.40 Oil objective. Time-lapse images were taken every 10 sec.

Movie 6: Curved filopodia and irregular cell fronts in tip cells of *sn* mutant

Live-imaging of DB tip cells of *sn* mutant (*sn^{P1};btlGal4>UASsrcGFP*) was acquired using an inverted TCS-SP5 confocal microscope with a 63.0x1.40 Oil objective. Time-lapse images were taken every 10 sec, revealing bent and flaccid filopodia, that often extend parallel to the irregular and disorganised cell front.

Movie 7: Organised actin dynamics in wild-type tip cells.

Utr-GFP in an otherwise wild-type background was visualised in an inverted Zeiss Lsm780 confocal with 63x Water objective and a 1,6 zoom. Images were taken every 13,56 and 14,04 seconds in 5-6µm Z-stack. Note the high and linear accumulation of actin that organises towards the protruding front of the leading cells (lamellipodium) and that reaches out at least until the base of the straight filopodia. Long bundles of actin extend from the cytoplasmic meshwork and reorganise to form the filopodia.

Movie 8: Disorganised actin cytoskeleton in *sn* mutant tip cells

Time-lapse imaging of Utr-GFP expressed in *sn* mutant cells, visualised in an inverted Zeiss Lsm780 confocal with 63x Water objective and a 1,8 zoom. Images were taken every 14,04 seconds in 5-6µm Z-stack. Actin accumulation appears in very short bundles or as punctae that moves apparently randomly trough the cytoplasm and that do not organise in a continuous and dense network at the lamellipodium. Note that filopodia form without detectable long and cytoplasmic-organised bundles of actin.

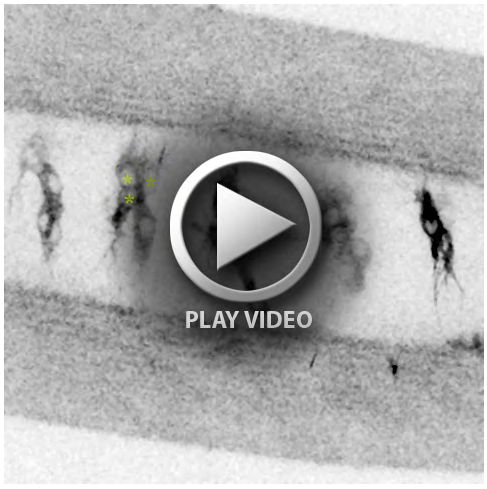

Movie 9: Live-imaging of dorsal branches overexpressing a non-phosphorytable form of Sn (Sn^{S52A})

Embryo expressing *sn^{S52A}-GFP* under the *btlGal4* driver was visualized using an inverted TCS-SP5 confocal microscope with a 63.0x1.40 Oil objective. Time-lapse images were taken every 1min14sec. Note the presence of extra tip cells (yellow asterisks, three tip-cells instead of 2 in normal conditions.). Note the thick and robust cytoplasmic extensions of terminal cells (magenta arrowhead), which clearly display straight and thick filopodia.

Movie 10 (Figure 6D): Subcellular localisation of a non-phosphorytable form of Sn (Sn^{S52A}) in tip cells

Images of tracheal tip cells from a *sn* mutant embryo (*sn^{P1}*) carrying *btlGal4>UASSn^{S52A}-GFP* visualised using an inverted TCS-SP5 confocal microscope with a 63.0x1.40 Oil objective. Frames were taken every 10sec, revealing an enrichment of Sn^{S52A} in the filopodia, although it is also present in the cytoplasm.

Movie 11 (Figure 6E)*:* Subcellular localisation of a phosphomimetic form of Sn (Sn^{S52E}) in tip cells

Images of tracheal tip cells from a *sn* mutant embryo (*sn^{P1}*) carrying *btlGal4>UASSn^{S52E}-GFP* visualised using an inverted TCS-SP5 confocal microscope with a 63.0x1.40 Oil objective. Frames were taken every 10sec, showing a diffuse accumulation of Sn^{S52E} throughout the cytoplasm, although it also appears transiently in filopodia.

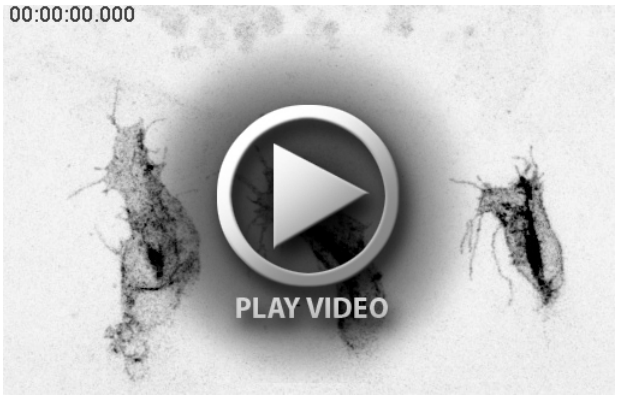

Movie 12 (Figure 7H): *sn* and *f* double mutant fast time-lapse imaging of filopodia and tip cell shape

Live-imaging of DB tip cells of $sn^{3}f^{36a}$ mutant ($sn^{3}f^{36a}$;*btlGal4>UASsrcGFP*) was acquired using an inverted TCS-SP5 confocal microscope with a 63.0x1.40 Oil objective. Time-lapse images were taken every 10sec, showing only few, short and sometimes bent filopodia, arising from very irregular and unproductive cell fronts.

Movie 13 (Figure 7I): Fast time-lapse imaging of filopodia and tip cell shape of a *sn* and *f* double mutant expressing wild-type Sn in the trachea

Live-imaging of DB tip cells of a $sn^{3}f^{36a}$ mutant carrying *btlGal4>UASsn-GFP* was acquired using an inverted TCS-SP5 confocal microscope with a 63.0x1.40 Oil objective. Time-lapse images were taken every 10sec, and show a clear rescue of the straightness of filopodia and of the irregular cell fronts of double mutants.